Strål
säkerhets
myndigheten
Swedish Radiation Safety Authority

Authors: Jeoung Seok Yoon[1], Ove Stephansson[1] and Ki-Bok Min[2]
[1] Stephansson Rock Consultant, Berlin, Germany
[2] Seoul National University, Seoul, South Korea

Technical Note 74; page 191-220

2014:59

Relation between earthquake magnitude, fracture length and fracture shear displacement in the KBS-3 repository at Forsmark

Main Review Phase

Date: December 2014
Report number: 2014:59 **ISSN:** 2000-0456
Available at www.stralsakerhetsmyndigheten.se

Models in Section 6.4

Earthquake induced, ZFMA2, present day reverse stress field, DFN03v

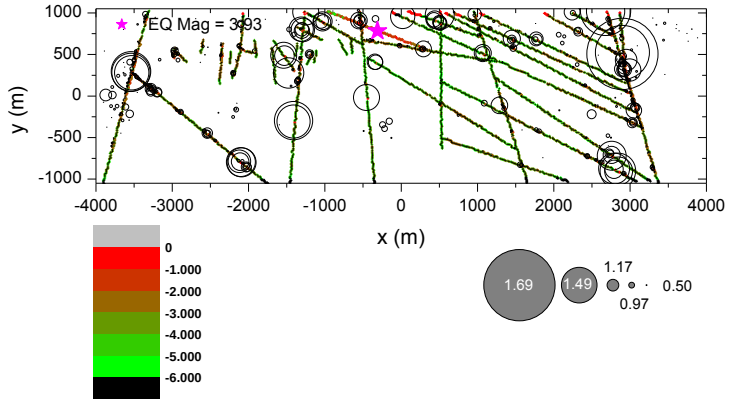

Figure A3-117. Spatial distribution of the induced seismic events and shear displacement of the joint planes that constitute the TFs and DZs, due to seismic event at zone ZFMA2 with realization DFN03v.

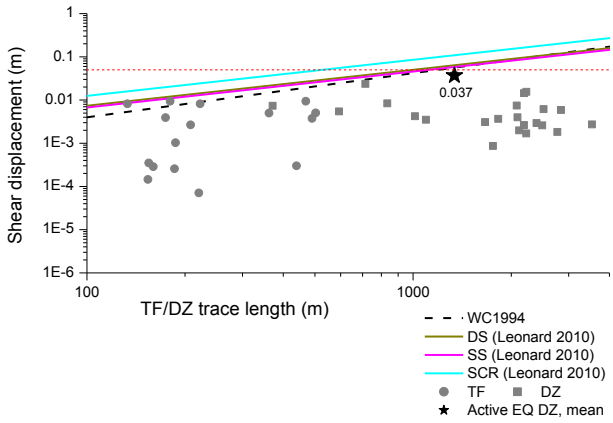

Figure A3-118. Shear displacement of the TFs and DZs with respect to length, due to seismic event at zone ZFMA2 with realization DFN03v and comparison with empirical regressions.

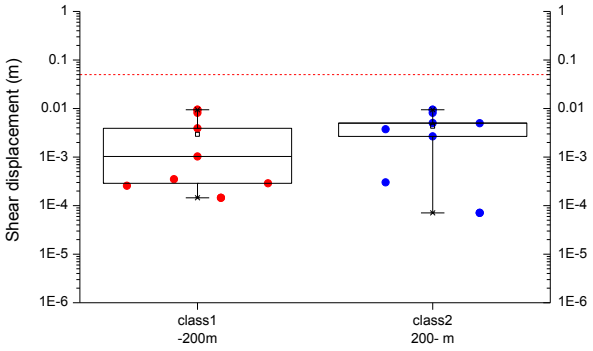

Figure A3-119. Box-and-whisker diagram of the TF shear displacement in four trace length classes, due to seismic event at zone ZFMA2 with realization DFN03v.

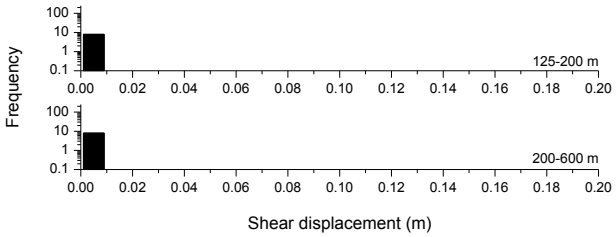

Figure A3-120. Histogram of shear displacement of the TFs in four different trace length classes, due to seismic event at zone ZFMA2 with realization DFN03v.

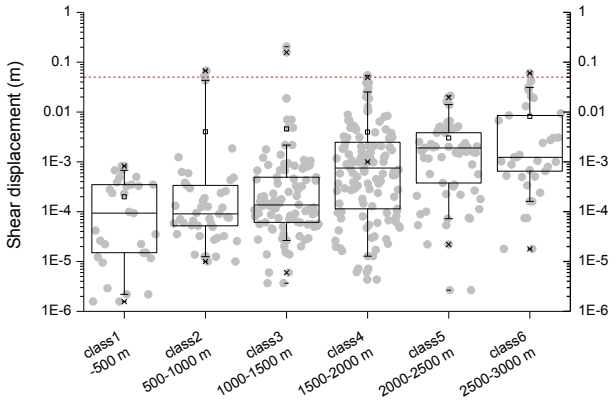

Figure A3-121. Box-and-whisker diagram of the shear displacement of smooth joints of TFs in six classes of distance from the hypocentre of the simulated earthquake.

Earthquake induced, ZFMA2, present day reverse stress field, DFN06v

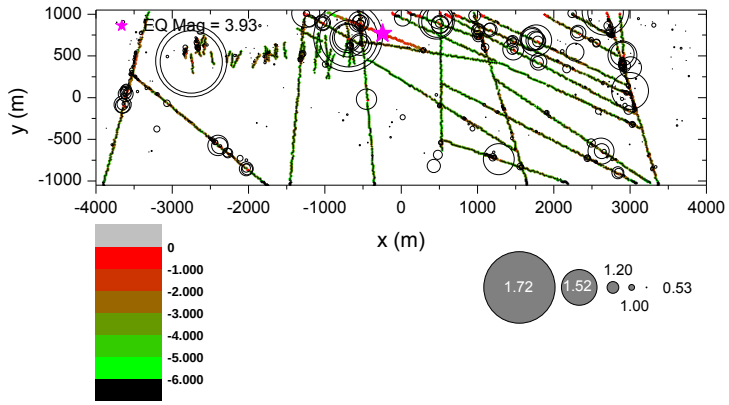

Figure A3-122. Spatial distribution of the induced seismic events and shear displacement of the joint planes that constitute the TFs and DZs, due to seismic event at zone ZFMA2 with realization DFN06v.

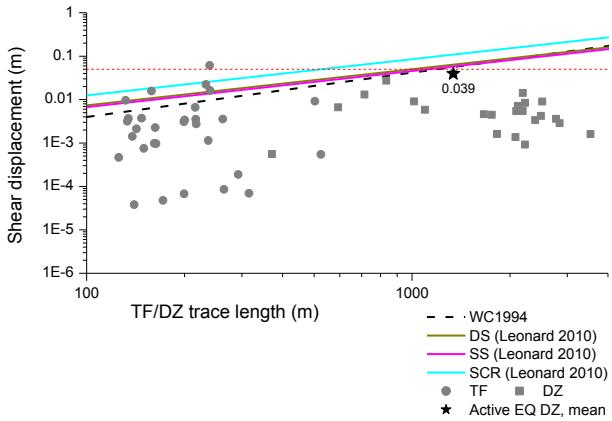

Figure A3-123. Shear displacement of the TFs and DZs with respect to length, due to seismic event at zone ZFMA2 with realization DFN06v and comparison with empirical regressions.

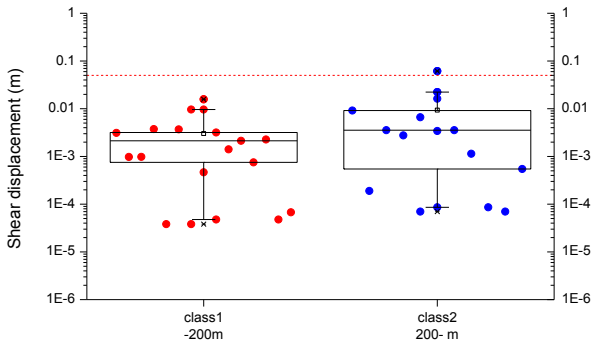

Figure A3-124. Box-and-whisker diagram of the TF shear displacement in four trace length classes, due to seismic event at zone ZFMA2 with realization DFN06v.

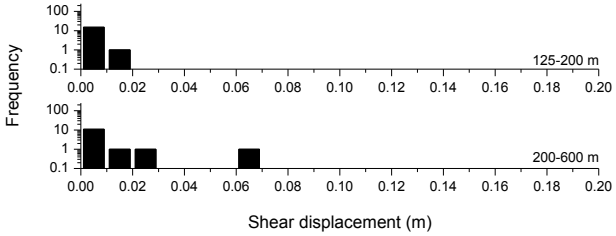

Figure A3-125. Histogram of shear displacement of the TFs in four different trace length classes, due to seismic event at zone ZFMA2 with realization DFN06v.

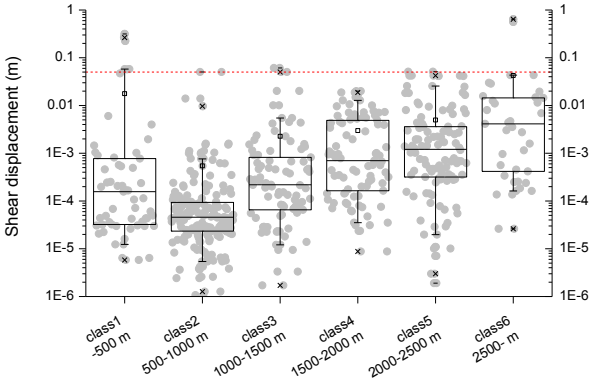

Figure A3-126. Box-and-whisker diagram of the shear displacement of smooth joints of TFs in six classes of distance from the hypocentre of simulated earthquake.

Earthquake induced, ZFMA2-A3-A8-F1, reverse stress field, DFN06v

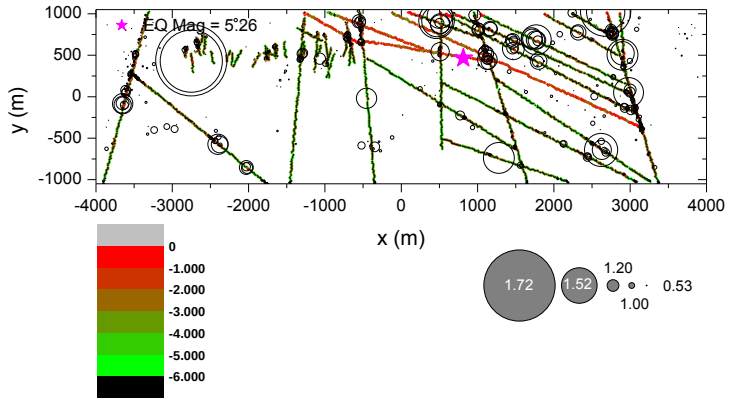

Figure A3-127. Spatial distribution of the induced seismic events and shear displacement of the joint planes that constitute the TFs and DZs, due to seismic event at zone ZFMA2-A3-A8-F1 with realization DFN06v.

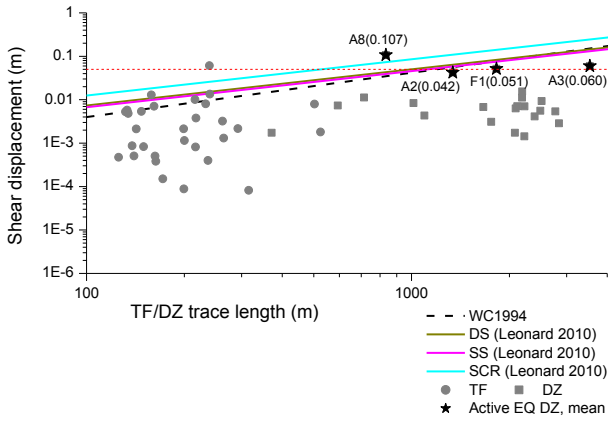

Figure A3-128. Shear displacement of the TFs and DZs with respect to length, due to seismic event at zone ZFMA2-A3-A8-F1 with realization DFN06v and comparison with empirical regressions.

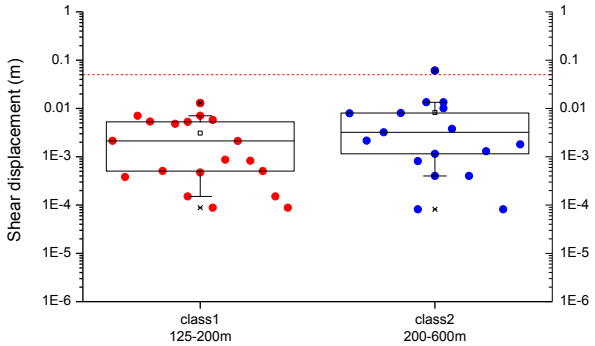

Figure A3-129. Box-and-whisker diagram of the TF shear displacement in four trace length classes, due to seismic event at zone ZFMA2-A3-A8-F1 with realization DFN06v.

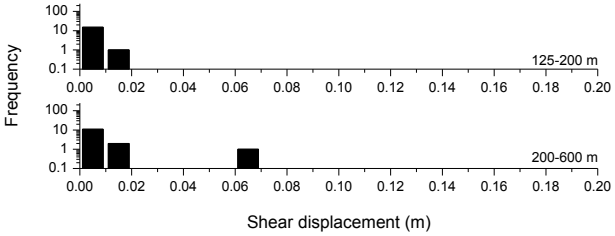

Figure A3-130. Histogram of shear displacement of the TFs in four different trace length classes, due to seismic event at zone ZFMA2-A3-A8-F1 with realization DFN06v.

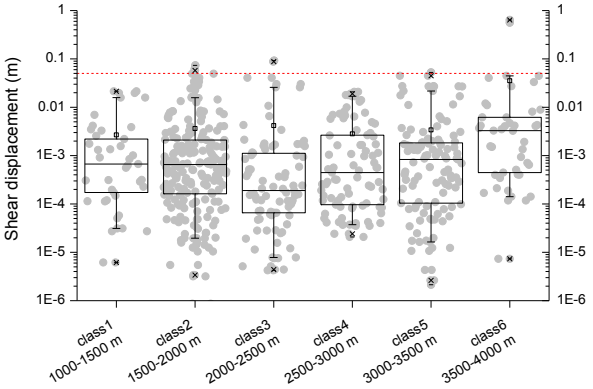

Figure A3-131. Box-and-whisker diagram of the shear displacement of smooth joints of TFs in six classes of distance from the hypocentre of simulated earthquake.

Earthquake induced, ZFMA2-A3-A8-F1, present day reverse stress field, DFN06v, powered shear force

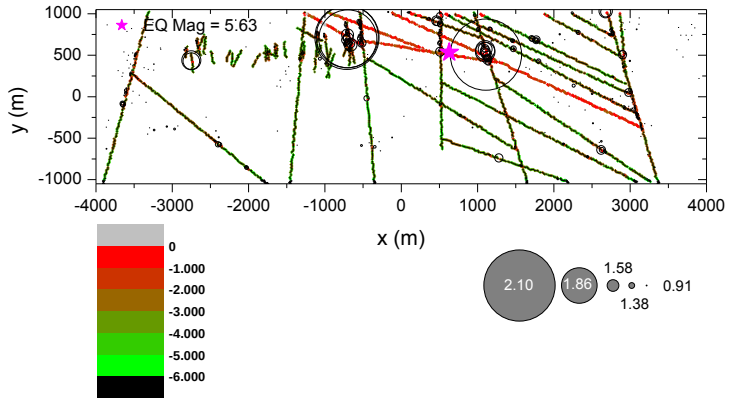

Figure A3-132. Spatial distribution of the induced seismic events and shear displacement of the joint planes that constitute the TFs and DZs, due to seismic event at zone ZFMA2-A3-A8-F1 with realization DFN06v.

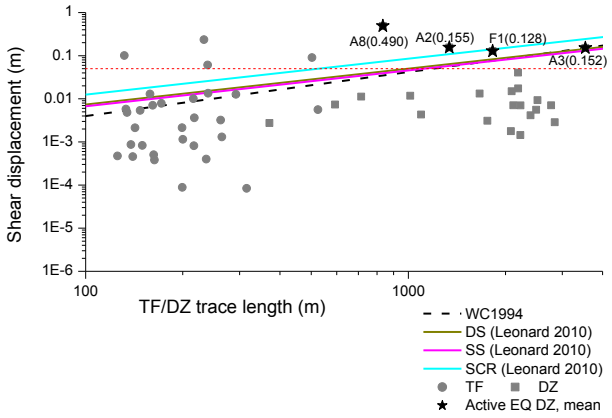

Figure A3-133. Shear displacement of the TFs and DZs with respect to length, due to seismic event at zone ZFMA2-A3-A8-F1 with realization DFN06v and comparison with empirical regressions.

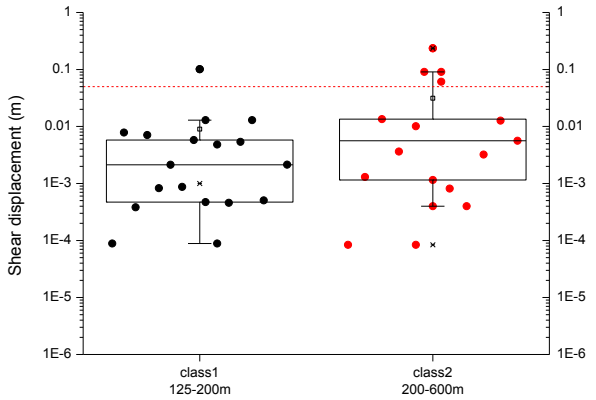

Figure A3-134. Box-and-whisker diagram of the TF shear displacement in four trace length classes, due to seismic event at zone ZFMA2-A3-A8-F1 with realization DFN06v.

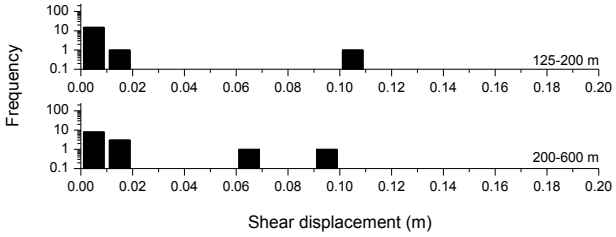

Figure A3-135. Histogram of shear displacement of the TFs in four different trace length classes, due to seismic event at zone ZFMA2-A3-A8-F1 with realization DFN06v.

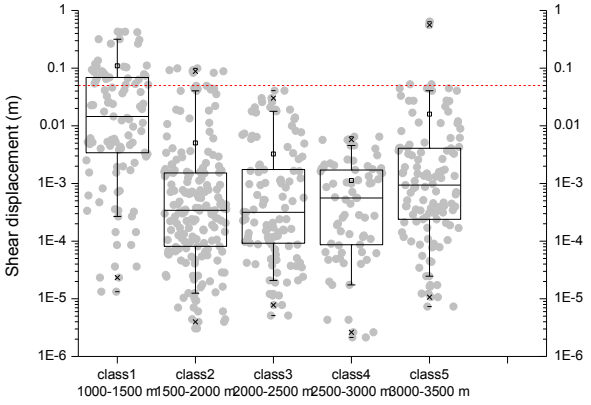

Figure A3-136. Box-and-whisker diagram of the shear displacement of smooth joints of TFs in five classes of distance from the hypocentre of simulated earthquake.

Models in Section 6.5

Earthquake induced, ZFMA2, glacial induced stress field at the time of maximum thickness of ice cover, DFN06v

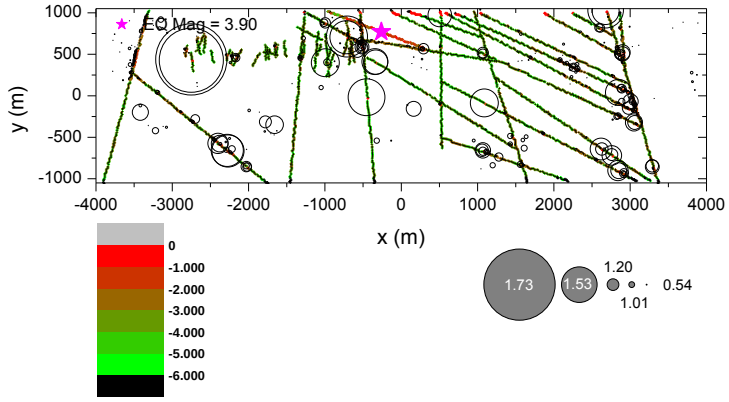

Figure A3-137. Spatial distribution of the induced seismic events and shear displacement of the joint planes that constitute the TFs and DZs, due to seismic event at zone ZFMA2 with realization DFN06v.

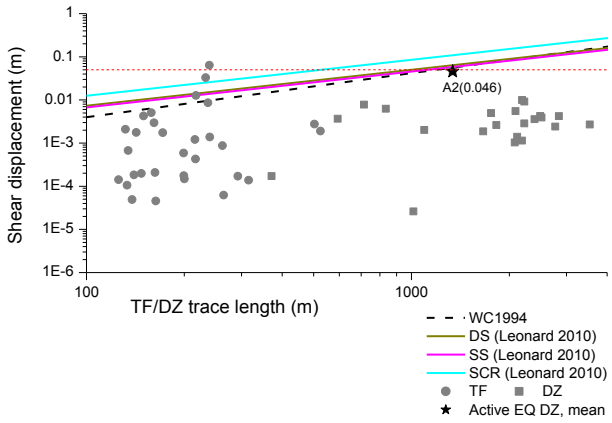

Figure A3-138. Shear displacement of the TFs and DZs with respect to length, due to seismic event at zone ZFMA2 with realization DFN06v and comparison with empirical regressions.

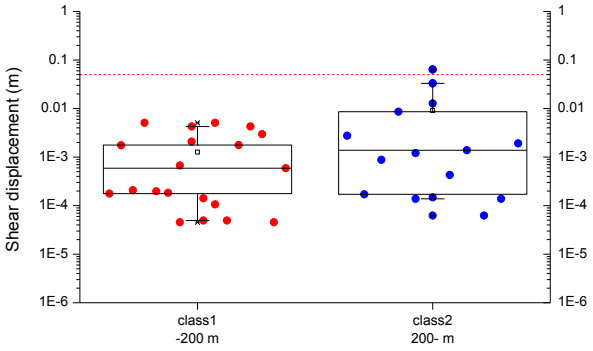

Figure A3-139. Box-and-whisker diagram of the TF shear displacement in four trace length classes, due to seismic event at zone ZFMA2 with realization DFN06v.

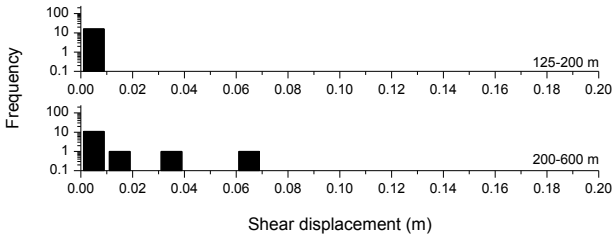

Figure A3-140. Histogram of shear displacement of the TFs in four different trace length classes, due to seismic event at zone ZFMA2 with realization DFN06v.

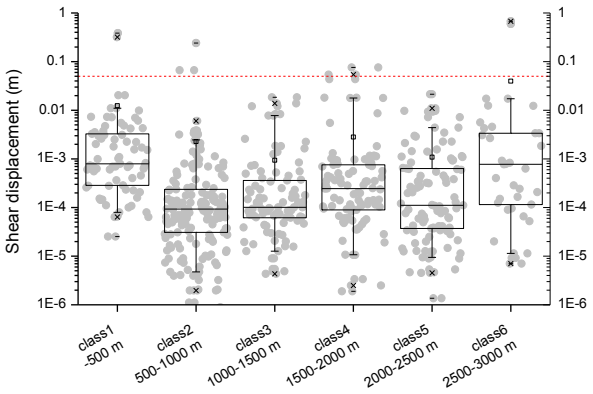

Figure A3-141. Box-and-whisker diagram of the shear displacement of smooth joints of TFs in six classes of distance from the hypocentre of simulated earthquake.

Earthquake induced, ZFMA2-A3-A8-F1, glacial induced stress field at the time of maximum thickness of ice cover, DFN06v

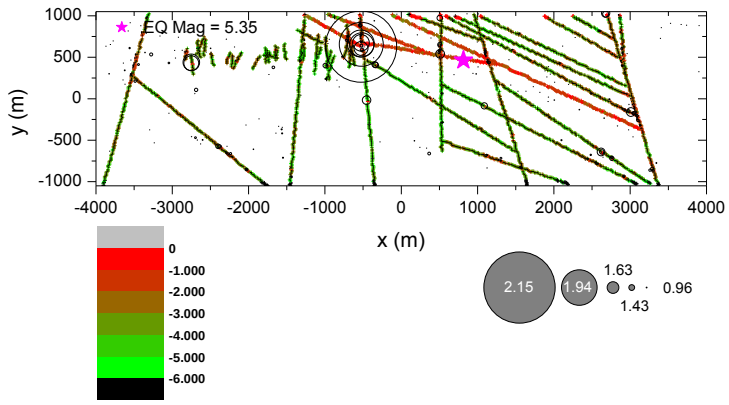

Figure A3-142. Spatial distribution of the induced seismic events and shear displacement of the joint planes that constitute the TFs and DZs, due to seismic event at zone ZFMA2-A3-A8-F1 with realization DFN06v.

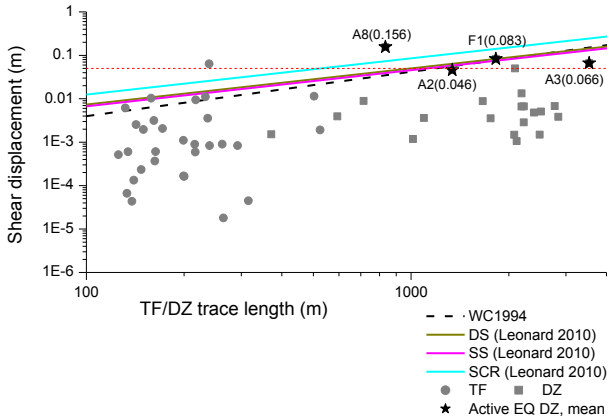

Figure A3-143. Shear displacement of the TFs and DZs with respect to the trace length, due to seismic event at zone ZFMA2-A3-A8-F1 with realization DFN06v and comparison with empirical regressions.

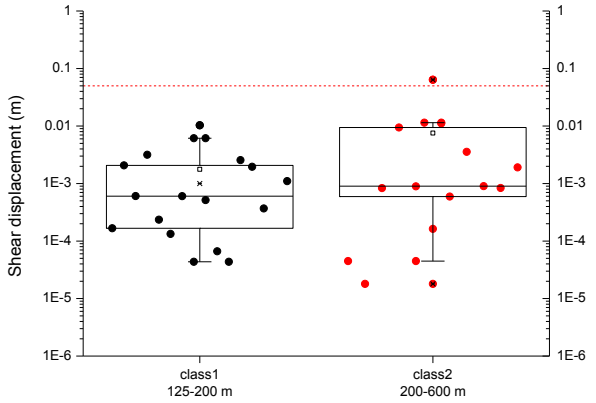

Figure A3-144. Box-and-whisker diagram of the TF shear displacement in four trace length classes, due to seismic event at zone ZFMA2-A3-A8-F1 with realization DFN06v.

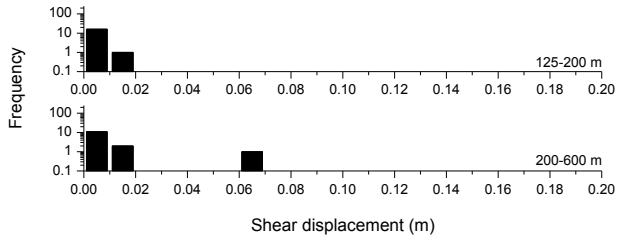

Figure A3-145. Histogram of shear displacement of the TFs in four different trace length classes, due to seismic event at zone ZFMA2-A3-A8-F1 with realization DFN06v.

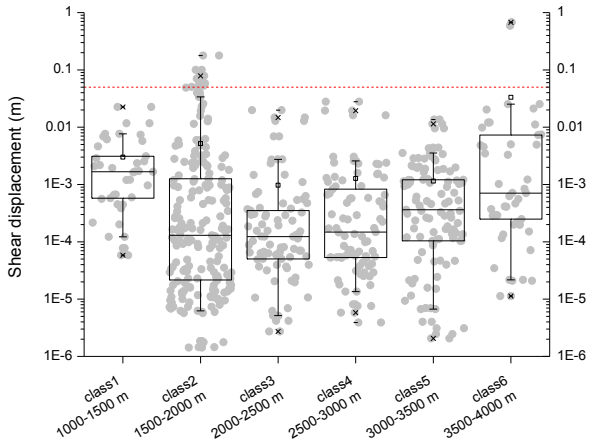

Figure A3-146. Box-and-whisker diagram of the shear displacement of smooth joints of TFs in six classes of distance from the hypocentre of simulated earthquake.

Earthquake induced, ZFMA2-A3-A8-F1, glacial induced stress field at the time of maximum thickness of ice cover, DFN06v, powered shear force

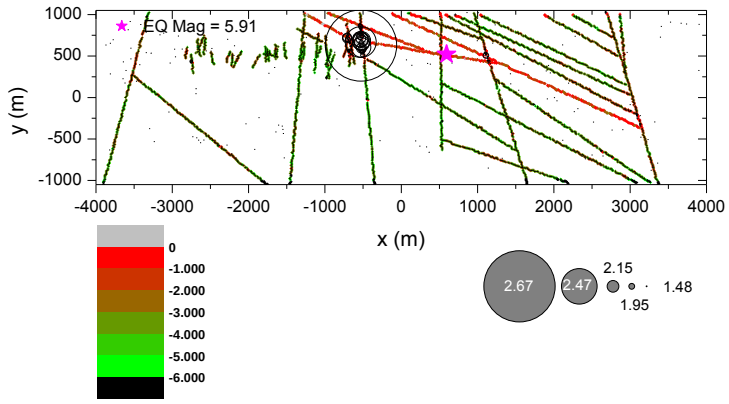

Figure A3-147. Spatial distribution of the induced seismic events and shear displacement of the joint planes that constitute the TFs and DZs, due to seismic event at zone ZFMA2-A3-A8-F1 with realization DFN06v.

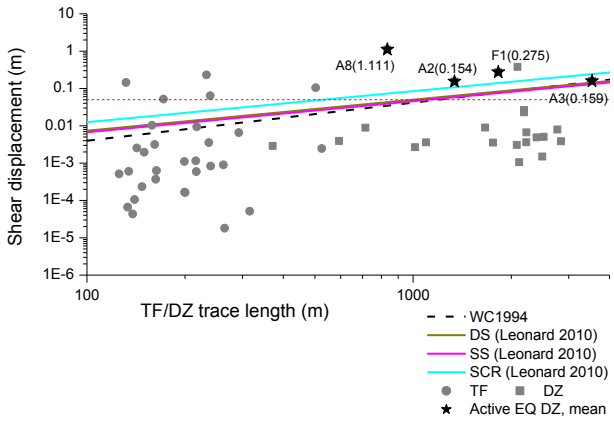

Figure A3-148. Shear displacement of the TFs and DZs with respect to length, due to seismic event at zone ZFMA2-A3-A8-F1 with realization DFN06v and comparison with empirical regressions.

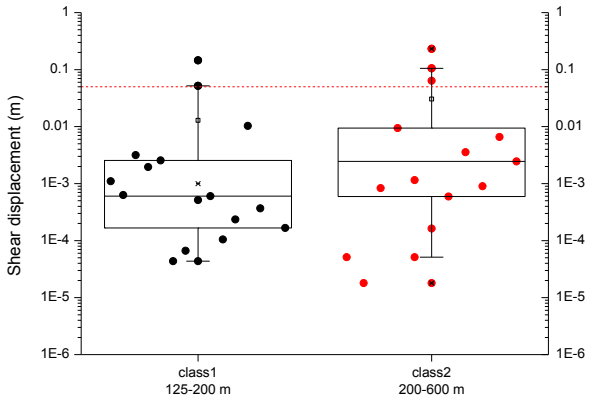

Figure A3-149. Box-and-whisker diagram of the TF shear displacement in four trace length classes, due to seismic event at zone ZFMA2-A3-A8-F1 with realization DFN06v.

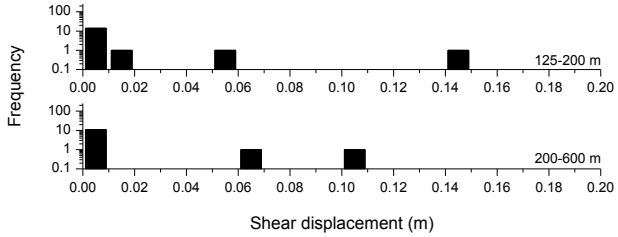

Figure A3-150. Histogram of shear displacement of the TFs in four different trace length classes, due to seismic event at zone ZFMA2-A3-A8-F1 with realization DFN06v.

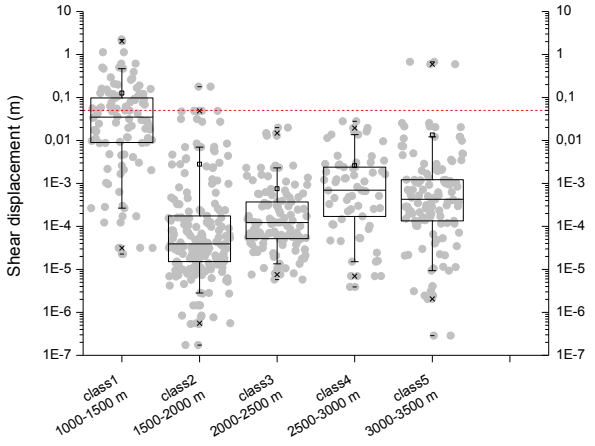

Figure A3-151. Box-and-whisker diagram of the shear displacement of smooth joints of TFs in five classes of distance from the hypocentre of simulated earthquake.

Models in Section 6.6

Earthquake induced, ZFMA2, glacial induced stress field at the time of ice retreat, DFN06v

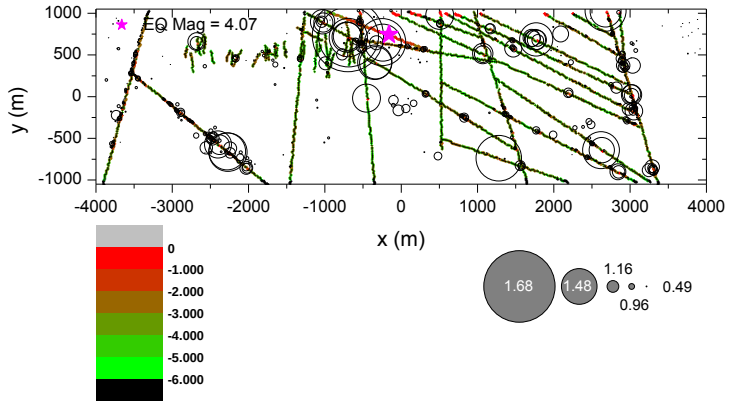

Figure A3-152. Spatial distribution of the induced seismic events and shear displacement of the joint planes that constitute the TFs and DZs, due to seismic event at zone ZFMA2 with realization DFN06v.

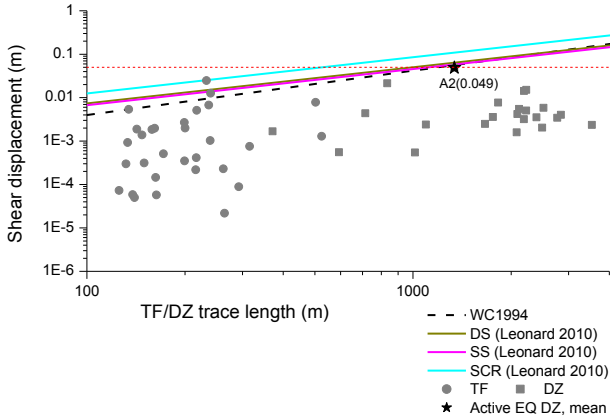

Figure A3-153. Shear displacement of the TFs and DZs with respect to length, due to seismic event at zone ZFMA2 with realization DFN06v and comparison with empirical regressions.

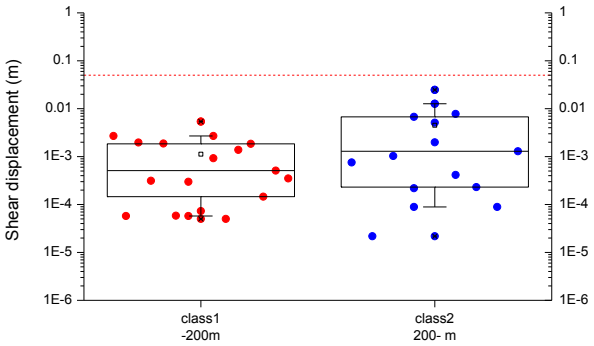

Figure A3-154. Box-and-whisker diagram of the TF shear displacement in four trace length classes, due to seismic event at zone ZFMA2 with realization DFN06v.

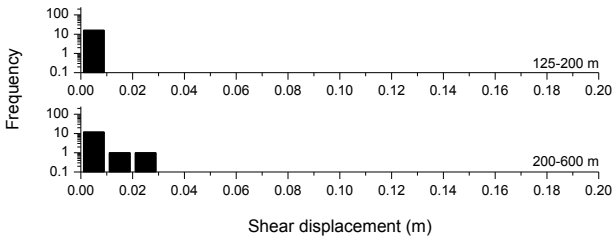

Figure A3-155. Histogram of shear displacement of the TFs in four different trace length classes, due to seismic event at zone ZFMA2 with realization DFN06v.

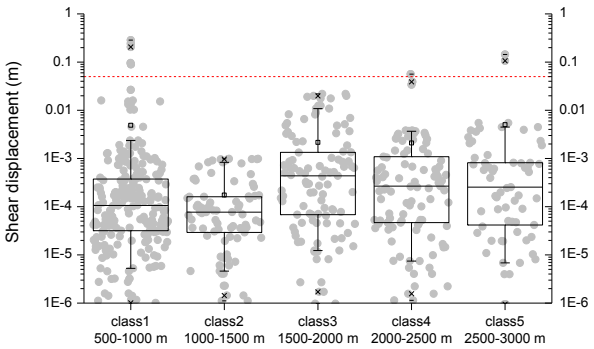

Figure A3-156. Box-and-whisker diagram of the shear displacement of smooth joints of TFs in five classes of distance from the hypocentre of simulated earthquake.

Earthquake induced, ZFMA2-A3-A8-F1, glacial induced stress field at the time of ice retreat, DFN03v

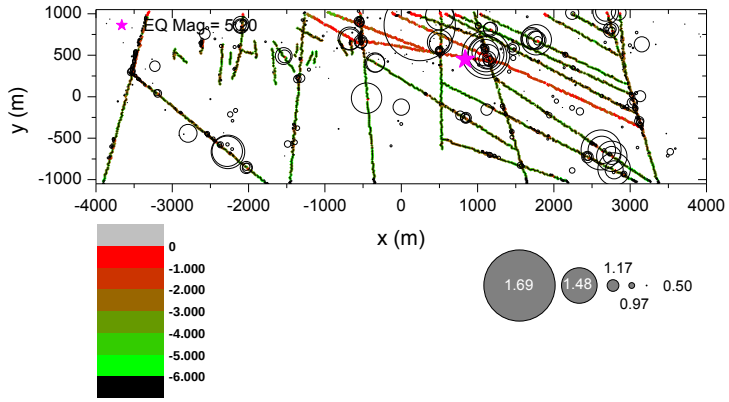

Figure A3-157. Spatial distribution of the induced seismic events and shear displacement of the joint planes that constitute the TFs and DZs, due to seismic event at zone ZFMA2-A3-A8-F1 with realization DFN03v.

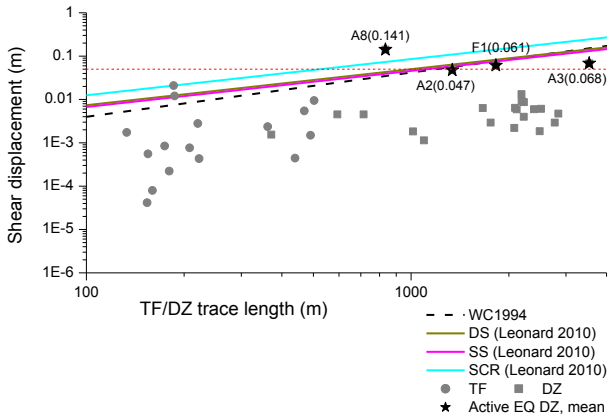

Figure A3-158. Shear displacement of the TFs and DZs with respect to length, due to seismic event at zone ZFMA2-A3-A8-F1 with realization DFN03v and comparison with empirical regressions.

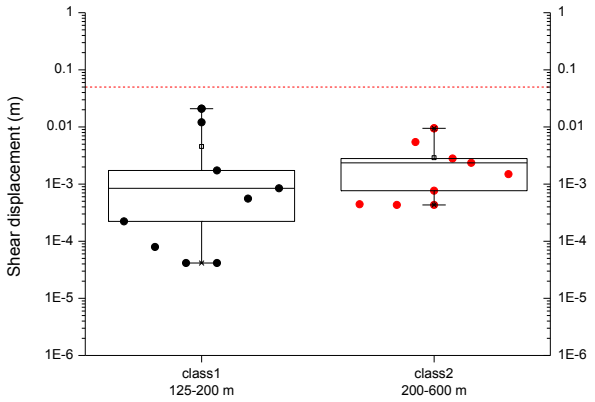

Figure A3-159. Box-and-whisker diagram of the TF shear displacement in four trace length classes, due to seismic event at zone ZFMA2-A3-A8-F1 with realization DFN03v.

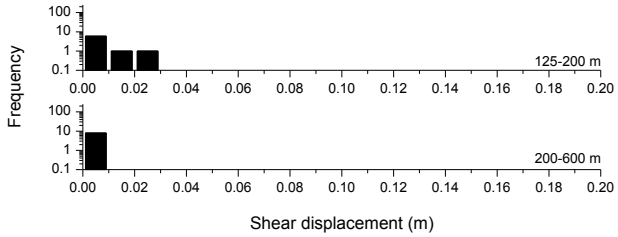

Figure A3-160. Histogram of shear displacement of the TFs in four different trace length classes, due to seismic event at zone ZFMA2-A3-A8-F1 with realization DFN03v.

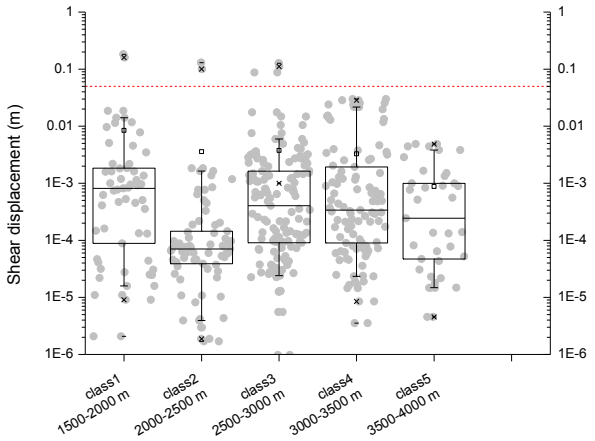

Figure A3-161. Box-and-whisker diagram of the shear displacement of smooth joints of TFs in five classes of distance from the hypocentre of simulated earthquake.

Earthquake induced, ZFMA2-A3-A8-F1, glacial induced stress field at the time of ice retreat, DFN06v

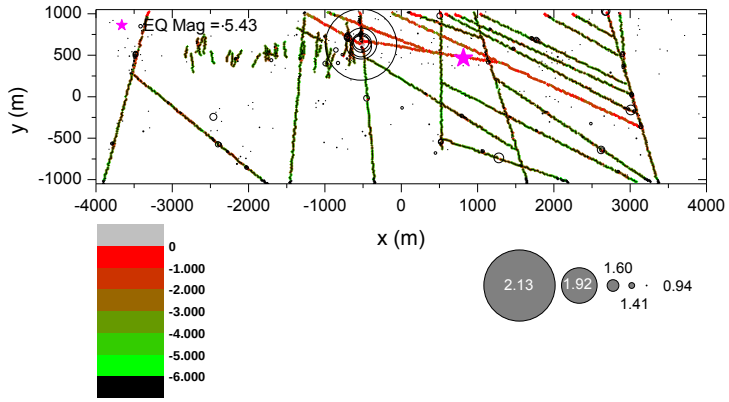

Figure A3-162. Spatial distribution of the induced seismic events and shear displacement of the joint planes that constitute the TFs and DZs, due to seismic event at zone ZFMA2-A3-A8-F1 with realization DFN06v.

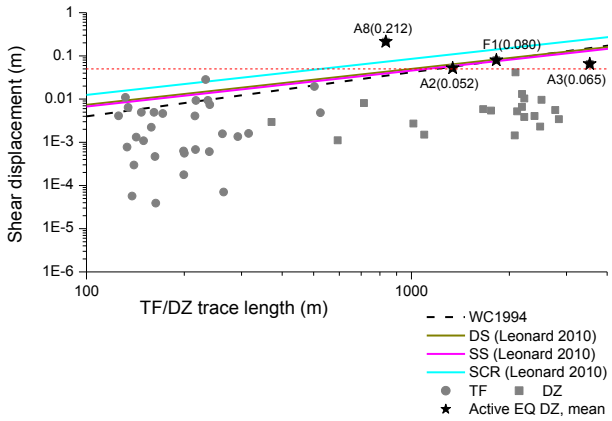

Figure A3-163. Shear displacement of the TFs and DZs with respect to length, due to seismic event at zone ZFMA2-A3-A8-F1 with realization DFN06v and comparison with empirical regressions.

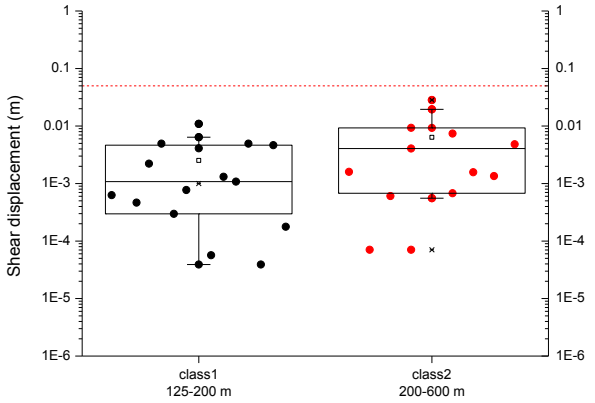

Figure A3-164. Box-and-whisker diagram of the TF shear displacement in four trace length classes, due to seismic event at zone ZFMA2-A3-A8-F1 with realization DFN06v.

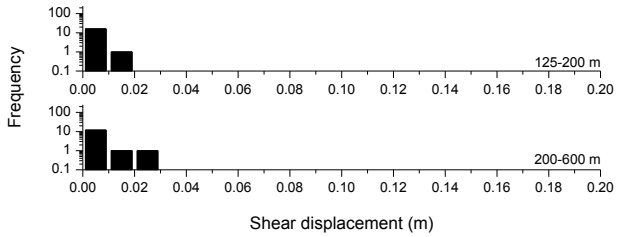

Figure A3-165. Histogram of shear displacement of the TFs in four different trace length classes, due to seismic event at zone ZFMA2-A3-A8-F1 with realization DFN06v.

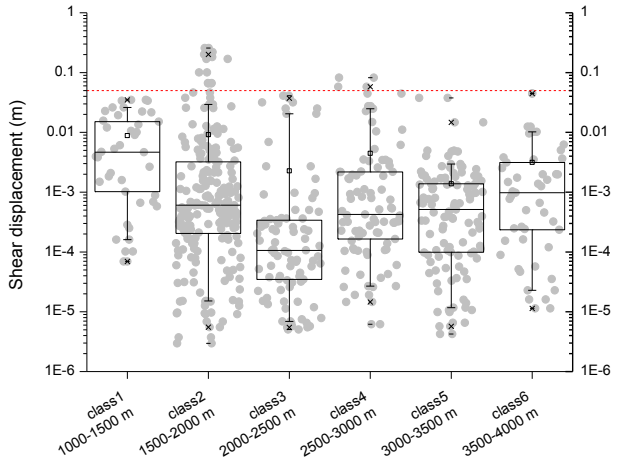

Figure A3-166. Box-and-whisker diagram of the shear displacement of smooth joints of TFs in six classes of distance from the hypocentre of simulated earthquake.

Earthquake induced, ZFMA2-A3-A8-F1, glacial induced stress field at time of ice retreat, DFN03v, powered shear force

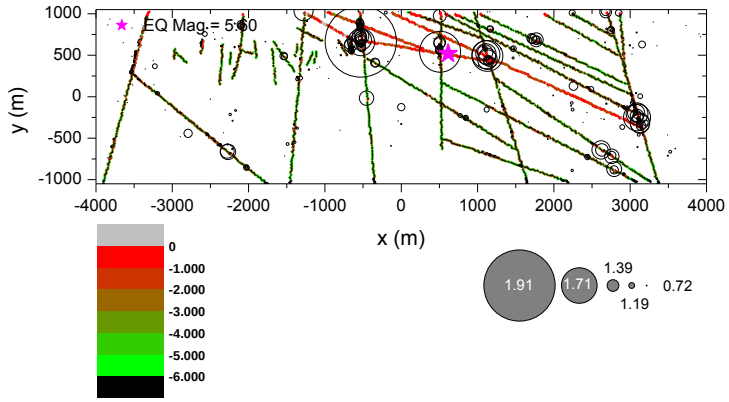

Figure A3-167. Spatial distribution of the induced seismic events and shear displacement of the joint planes that constitute the TFs and DZs, due to seismic event at zone ZFMA2-A3-A8-F1 with realization DFN03v.

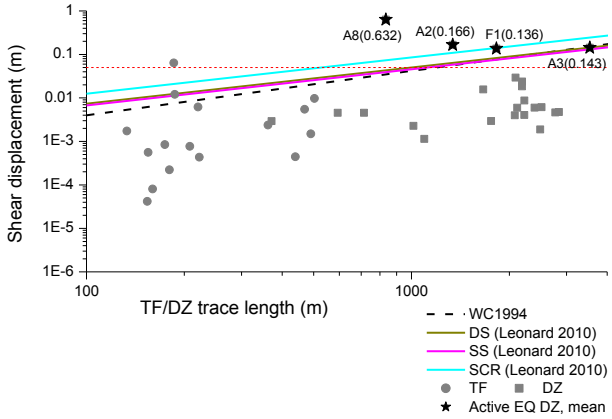

Figure A3-168. Shear displacement of the TFs and DZs with respect to length, due to seismic event at zone ZFMA2-A3-A8-F1 with realization DFN03v and comparison with empirical regressions.

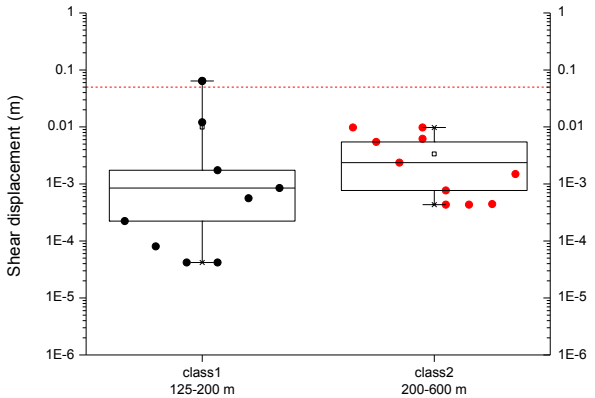

Figure A3-169. Box-and-whisker diagram of the TF shear displacement in four trace length classes, due to seismic event at zone ZFMA2-A3-A8-F1 with realization DFN03v.

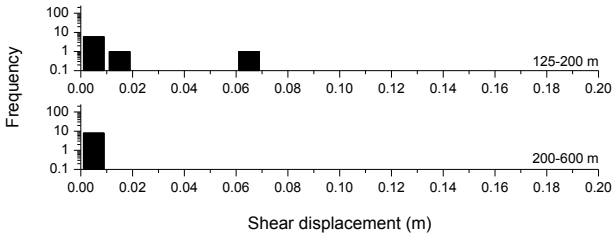

Figure A3-170. Histogram of shear displacement of the TFs in four different trace length classes, due to seismic event at zone ZFMA2-A3-A8-F1 with realization DFN03v.

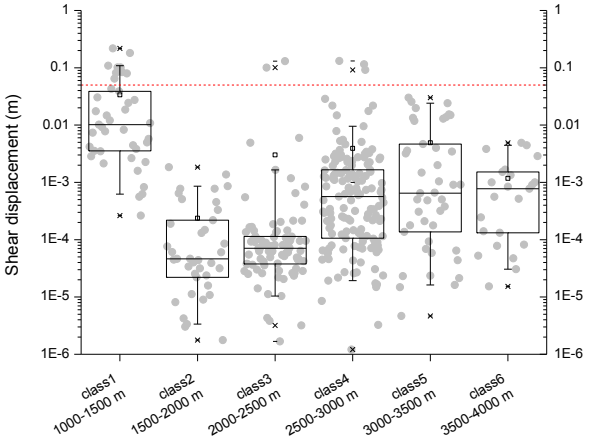

Figure A3-171. Box-and-whisker diagram of the shear displacement of smooth joints of TFs in six classes of distance from the hypocentre of simulated earthquake.

Earthquake induced, ZFMA2-A3-A8-F1, glacial induced stress field at the time of ice retreat, DFN06v, powered shear force

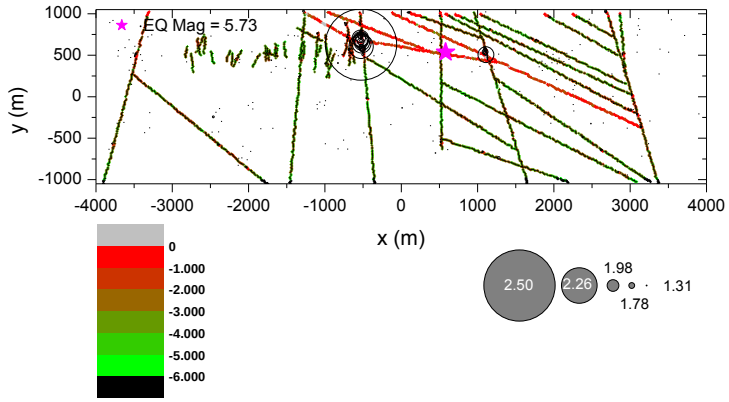

Figure A3-172. Spatial distribution of the induced seismic events and shear displacement of the joint planes that constitute the TFs and DZs, due to seismic event at zone ZFMA2-A3-A8-F1 with realization DFN06v.

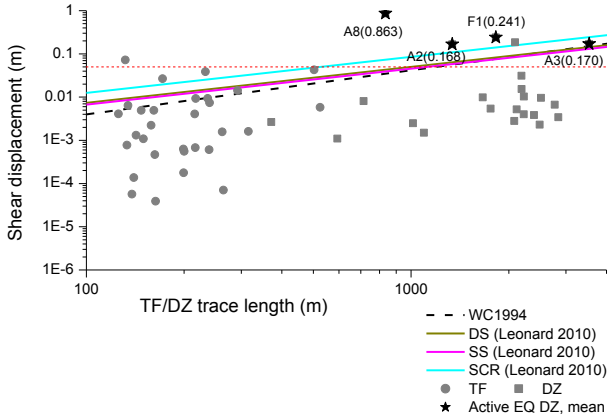

Figure A3-173. Shear displacement of the TFs and DZs with respect to length, due to seismic event at zone ZFMA2-A3-A8-F1 with realization DFN06v and comparison with empirical regressions.

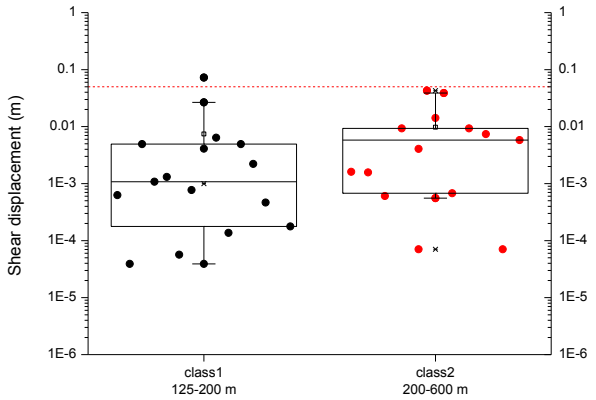

Figure A3-174. Box-and-whisker diagram of the TF shear displacement in four trace length classes, due to seismic event at zone ZFMA2-A3-A8-F1 with realization DFN06v.

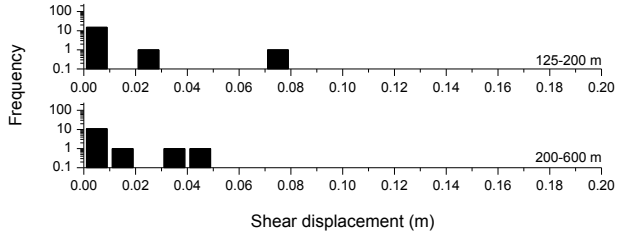

Figure A3-175. Histogram of shear displacement of the TFs in four different trace length classes, due to seismic event at zone ZFMA2-A3-A8-F1 with realization DFN06v.

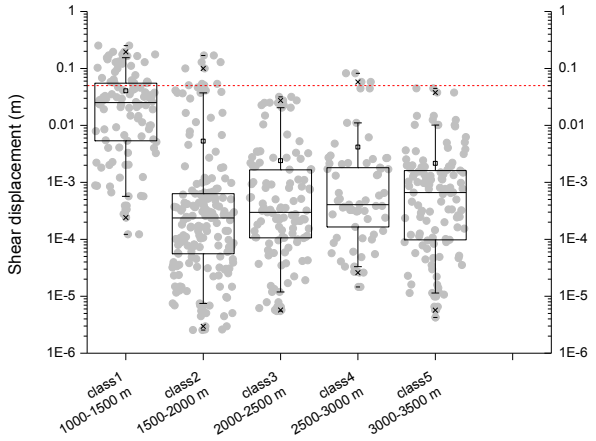

Figure A3-176. Box-and-whisker diagram of the shear displacement of smooth joints of TFs in five classes of distance from the hypocentre of simulated earthquake.

Models in Section 7.1

Thermal and earthquake induced, sequential heating, ZFMWNW0809A at 50y after start of heating, present day most likely stress, DFN03h

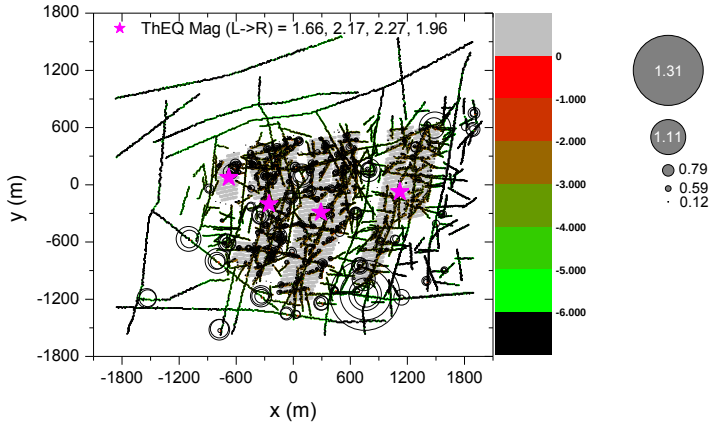

Figure A3-177. Spatial distribution of the thermally induced seismic events and shear displacement of the joint planes that constitute the TFs and DZs, due to 50 years of sequential heating with realization DFN03h.

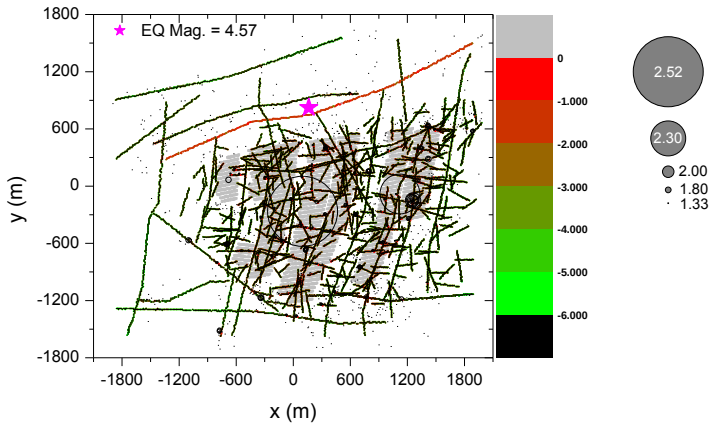

Figure A3-178. Spatial distribution of the earthquake (ZFMWNW0809A) induced seismic events and shear displacement of the joint planes that constitute the TFs and DZs superposed to 50 years of sequential heating with realization DFN03h.

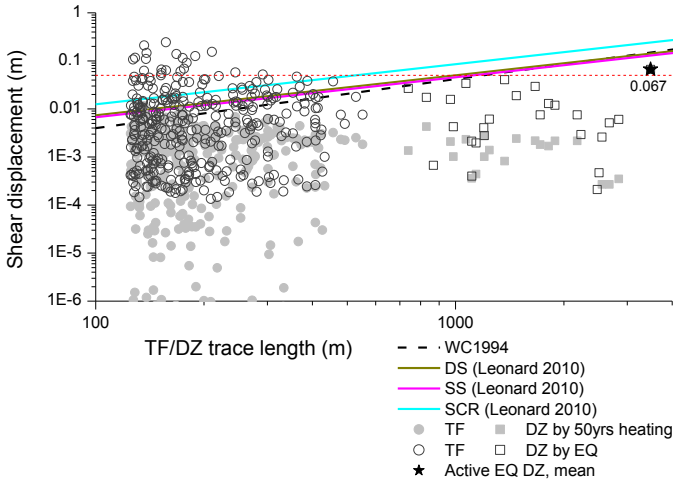

Figure A3-179. Shear displacement of the TFs and DZs with respect to length, due to earthquake (ZFMWNW0809A) superposed to 50 years of sequential heating with realization DFN03h.

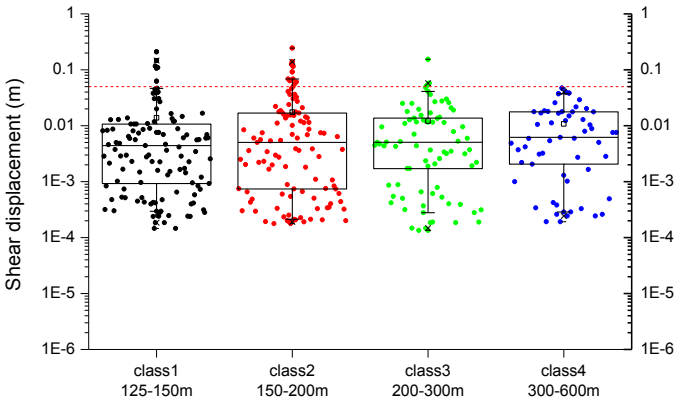

Figure A3-180. Box-and-whisker diagram of the TF shear displacement in four trace length classes, due to earthquake (ZFMWNW0809A) superposed to 50 years of sequential heating with realization DFN03h.

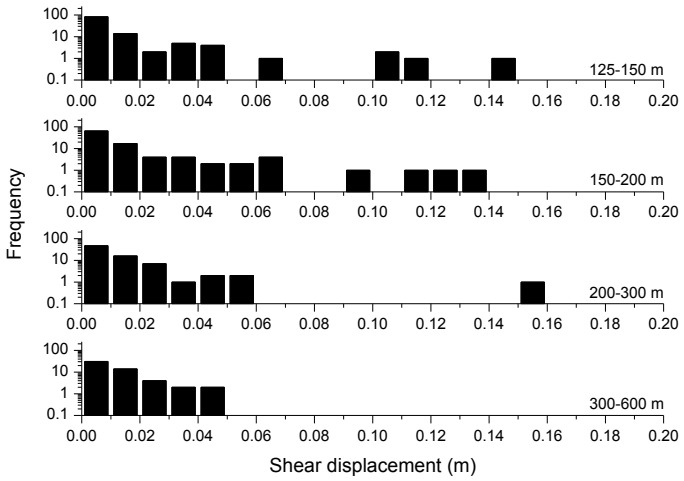

Figure A3-181. Histogram of shear displacement of the TFs in four different trace length classes, due to earthquake (ZFMWNW0809A) superposed to 50 years of sequential heating with realization DFN03h.

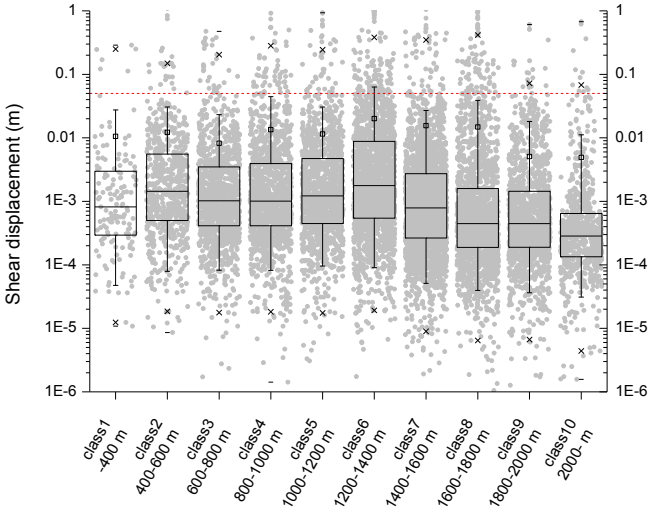

Figure A3-182. Box-and-whisker diagram of the shear displacement of smooth joints of TFs in ten classes of distance from the hypocentre of simulated earthquake.

Models in Section 7.2

Thermal and earthquake induced, sequential heating, ZFMWNW2225 at 50y after start of heating, present day most likely stress, DFN03h

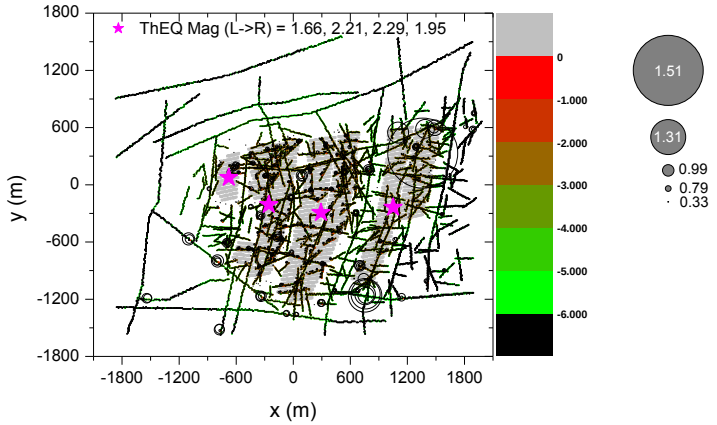

Figure A3-183. Spatial distribution of the thermally induced seismic events and shear displacement of the joint planes that constitute the TFs and DZs, due to 50 years of sequential heating with realization DFN03h.

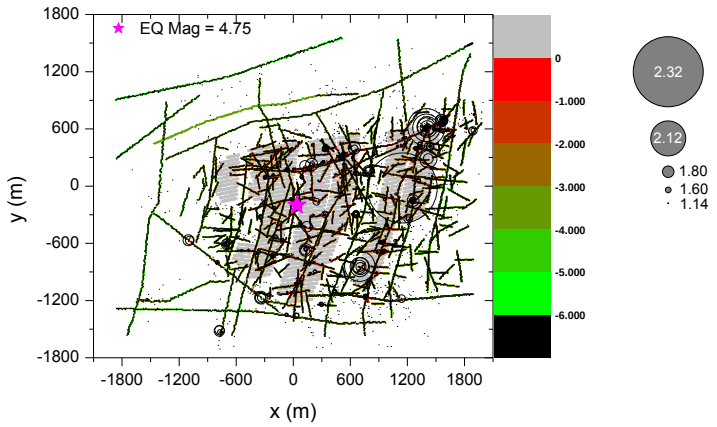

Figure A3-184. Spatial distribution of the earthquake (ZFMWNW2225) induced seismic events and shear displacement of the joint planes that constitute the TFs and DZs superposed to 50 years of sequential heating with realization DFN03h.

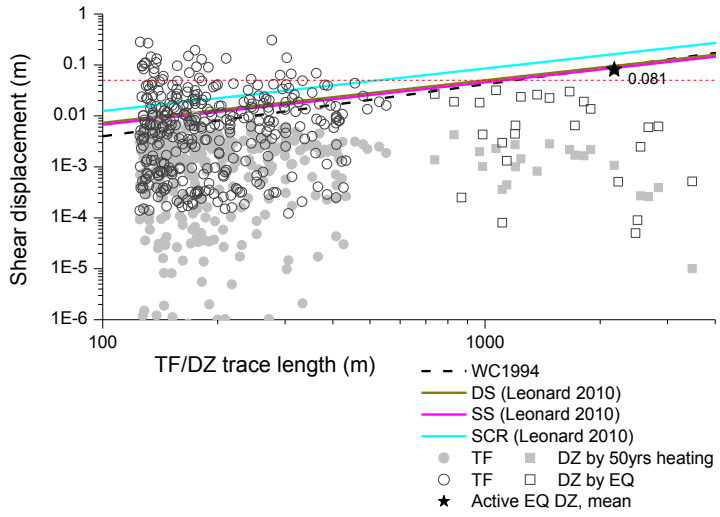

Figure A3-185. Shear displacement of the TFs and DZs with respect to length, due to earthquake (ZFMWNW2225) superposed to 50 years of sequential heating with realization DFN03h.

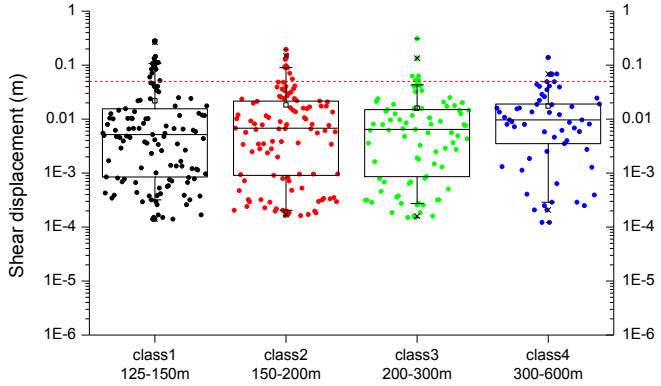

Figure A3-186. Box-and-whisker diagram of the TF shear displacement in four trace length classes, due to earthquake (ZFMWNW2225) superposed to 50 years of sequential heating with realization DFN03h.

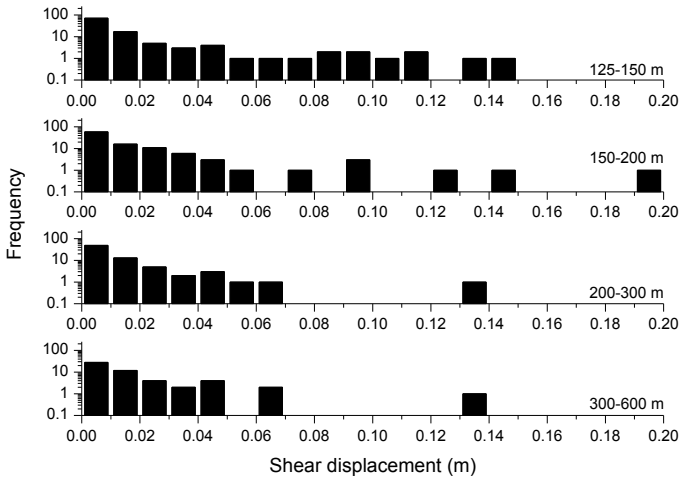

Figure A3-187. Histogram of shear displacement of the TFs in four different trace length classes, due to earthquake (ZFMWNW2225) superposed to 50 years of sequential heating with realization DFN03h.

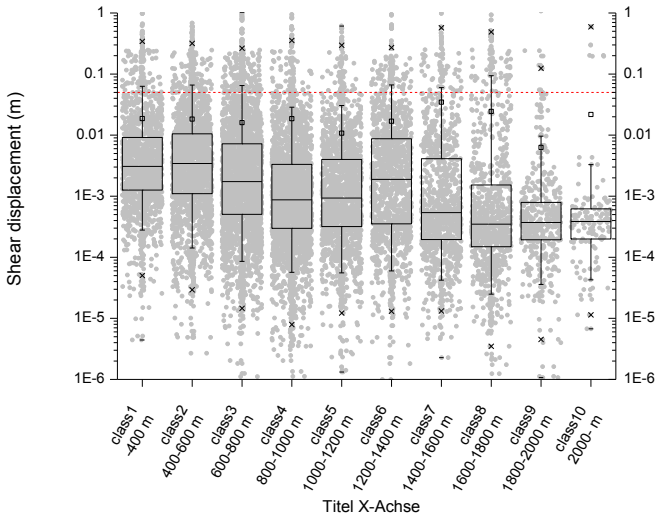

Figure A3-188. Box-and-whisker diagram of the shear displacement of smooth joints of TFs in ten classes of distance from the hypocentre of simulated earthquake.

2014:59

The Swedish Radiation Safety Authority has a comprehensive responsibility to ensure that society is safe from the effects of radiation. The Authority works to achieve radiation safety in a number of areas: nuclear power, medical care as well as commercial products and services. The Authority also works to achieve protection from natural radiation and to increase the level of radiation safety internationally.

The Swedish Radiation Safety Authority works proactively and preventively to protect people and the environment from the harmful effects of radiation, now and in the future. The Authority issues regulations and supervises compliance, while also supporting research, providing training and information, and issuing advice. Often, activities involving radiation require licences issued by the Authority. The Swedish Radiation Safety Authority maintains emergency preparedness around the clock with the aim of limiting the aftermath of radiation accidents and the unintentional spreading of radioactive substances. The Authority participates in international co-operation in order to promote radiation safety and finances projects aiming to raise the level of radiation safety in certain Eastern European countries.

The Authority reports to the Ministry of the Environment and has around 315 employees with competencies in the fields of engineering, natural and behavioural sciences, law, economics and communications. We have received quality, environmental and working environment certification.

Strålsäkerhetsmyndigheten
Swedish Radiation Safety Authority

SE-171 16 Stockholm
Solna strandväg 96

Tel: +46 8 799 40 00
Fax: +46 8 799 40 10

E-mail: registrator@ssm.se
Web: stralsakerhetsmyndigheten.se